Journal of Biomechanics 195 (2026) 113132

Contents lists available at ScienceDirect

Journal of Biomechanics

journal homepage: www.elsevier.com/locate/jbiomech

Assessment of fluid ingress into the graft-host interface of osteochondral grafts and synthetic scaffolds under cyclic axial loading in a tibio-femoral model

Lara Esquivel [a,*], Mingjing Zhang [b], Gavin Day [a], Marlène Mengoni [a], Hazel Fermor [c], Chaozong Liu [b], Ruth Wilcox [a]

[a] Institute of Medical & Biological Engineering, School of Mechanical Engineering, University of Leeds, UK
[b] Division of Surgery & Interventional Science, University College London, UK
[c] School of Biomedical Sciences, University of Leeds, UK

ARTICLE INFO

Keywords:
Osteochondral graft
Graft-host interface
Fluid movement
Cartilage repair
Subchondral bone cysts

ABSTRACT

This study developed an *in vitro* method to evaluate fluid ingress into the graft-host interface of osteochondral grafts and mimetic constructs and the risk of graft subsidence, using porcine and ovine tibio-femoral models, to investigate mechanisms associated with cyst development. Distal femurs were implanted with two osteochondral grafts or mimetic constructs. One was implanted axially with the loading direction at the point of initial contact of the femur and tibia ("loaded graft"); another on an unloaded portion of the opposite condyle ("unloaded graft"). During testing under a uniaxial cyclic loading regime, the specimens were housed in a contrast medium. Micro-CT scans taken before and after testing allowed the movement of the contrast fluid to be visualized. Fluid ingress was quantified by comparing the greyscale distribution across line profiles between the μCT scans. Ingress was calculated at six sites of interest: two at each graft site ("graft-host interface", "graft centre"), one through "loaded host bone", and one through "unloaded host bone". Graft presence and loading were key factors to promote fluid ingress ($p = 0.001$). Fluid ingress at loaded graft-host interfaces relative to the unloaded host bone of porcine-in-porcine was 2.4 ± 8.9 mm, porcine-in-ovine was 9.9 ± 3.1 mm, and mimetic constructs-inporcine was 3.6 ± 3.8 mm. A mismatch in material properties between the graft and host bone promoted ingress, driven by host bone quality. Subchondral bone damage and fluid pooling below grafts was detectable from μCT images. Results indicate host bone quality should be considered when assessing a patient's suitability for surgery.

1. Introduction

As articular cartilage has a limited ability to self-repair in adults (Davis et al., 2021), trauma or physiological changes can lead to the development of chondral and osteochondral lesions, which have the potential to progress into osteoarthritis. Options for the surgical repair of such lesions include marrow stimulation techniques (e.g. microfracture), autologous chondrocyte transplantation, and osteochondral grafting (Gao et al., 2020). In osteochondral grafting (allograft or autograft, mosaicplasty or single graft), local regions of cartilage damage are removed and replaced with healthy tissue or biomaterials, with the aim of re-establishing surface congruency and restoring joint biomechanics (Solanki et al., 2021). Osteochondral graft procedures have demonstrated good clinical outcomes, particularly for autologous grafts with success reported in 72 % of patients at 10 years post-surgery (Branam and Saber, 2023). Synthetic scaffolds are a promising off-the-shelf clinical alternative to natural grafts and demonstrate positive short and medium-term outcomes (Zeng et al., 2018). Synthetic scaffolds have the advantages of only requiring a single surgery and no donor site morbidity (Hoveidaei et al., 2024).

Reported failure mechanisms include non-integration of the graft with surrounding bone, delamination of the articular cartilage, advancing osteoarthritis, and cyst formation with subchondral bone necrosis and graft subsidence (Juels et al., 2020; Marom et al., 2020). Chondral and subchondral formation of fluid-filled sacks, or cysts, is associated with various cartilage treatment techniques (Beck et al.,

* Corresponding author at: Institute of Medical and Biological Engineering, School of Mechanical Engineering, University of Leeds, Woodhouse Lane, Woodhouse, Leeds LS29JT, UK.
E-mail address: mn20lse@leeds.ac.uk (L. Esquivel).

https://doi.org/10.1016/j.jbiomech.2025.113132
Accepted 14 December 2025
Available online 16 December 2025

2016; Gao et al., 2020). In osteochondral grafts, a 20 % prevalence of subchondral bone cysts was observed six months post-operatively (Ackermann et al., 2019b; Ackermann et al., 2019c) with reported incidences between 30 % and 80 % depending on the joint (Shimozono et al., 2018; Shimozono et al., 2019; Ackermann et al., 2019a).

The development of subchondral bone cysts has also been observed following cartilage treatment in several preclinical animal models including horses, rabbits, goats and sheep (Vachon et al., 1986; Chen et al., 2011; Pallante-Kichura et al., 2013; Beck et al., 2016). In sheep, a 92 % prevalence was observed six months post-operatively (Beck et al., 2016). With cyst presentation differing between species, a question arises concerning the respective influences of bone structure, specimen anatomy and mechanical properties on cyst formation, which differ widely between animal models (Oláh et al., 2021). For example, the bone mineral density of trabecular lumbar spine samples were reported as 178 mg/cm^3 in humans, 373 mg/cm^3 in pigs, and 437 mg/cm^3 in sheep (Aerssens et al., 1998). Local biomechanical overload has also been seen to contribute to the development of cysts (Wang et al., 2021).

Synovial fluid ingress, from the joint capsule into the graft-host interface and subchondral bone, has been theorised to induce inferior biomechanical and physiological conditions, contributing to an increased risk of cyst formation and contribution to graft failure (Pallante-Kichura et al., 2013; Ackermann, Merkely, et al., 2019; Gao et al., 2020; Solanki et al., 2021). However, currently there is little evidence on the level of fluid ingress at the graft-host interface or how this is affected by the graft and host bone properties, bony architecture or loading. Due to this gap in knowledge, there is a need for mechanistic studies to assess modes of cyst development. In particular, there is a lack of literature on fluid movement into subchondral bone to validate theories of cyst formation. Porcine and ovine models have previously been used in *in vitro* and *in vivo* tests for investigating osteochondral grafting (Bowland et al., 2019; Meng et al., 2020; Suderman et al., 2024). Given their differing bony architecture, then using the two species would allow investigation of the influence of bone structure with different graft types on fluid movement following osteochondral grafting.

The aim of this study was to develop a method to quantify fluid ingress and the risk of graft subsidence *in vitro*, and apply the method to evaluate natural and synthetic grafts in porcine and ovine tibiofemoral models.

2. Methods

2.1. Study Design

A method was developed to capture fluid ingress between graft and natural tissue sites in a tibiofemoral model following axial cyclic testing. The methods are described in detail below but briefly comprised the implantation of grafts into loaded and non-loaded regions of the tibiofemoral joint, cyclic axial loading of the specimen in the presence of a contrast medium, and imaging to measure fluid ingress and graft subsidence. Initial pilot studies were performed to iteratively change aspects of the cyclic testing procedure and to optimise post-processing methods (Supplementary Data – Section A, B). An overview of the experimental and post-processing methods is provided in Fig. 1.

Three types of specimens were used: natural porcine grafts in a porcine model, natural porcine grafts in an ovine model, and biomimetic synthetic constructs in a porcine model. These combinations were selected to capture a range of graft-host property combinations, representative of both clinical graft-host interface material mismatch and those used in pre-clinical *in vivo* testing.

2.2. Specimens

Natural osteochondral grafts consisted of a cylindrical plug of cartilage and subchondral bone (10 mm long and 6.5 mm diameter). These were harvested from the trochlear groove of porcine specimens with an Acufex™ Mosaicplasty surgical toolkit (Smith and Nephew, MA, USA).

A layered biomimetic construct comprising of a chondral-like upper layer and an osseous-like lower layer was designed to structurally replicate the architecture of natural osteochondral grafts (8 mm long and 7.5 mm diameter) (Zheng et al., 2022). This construct was provided

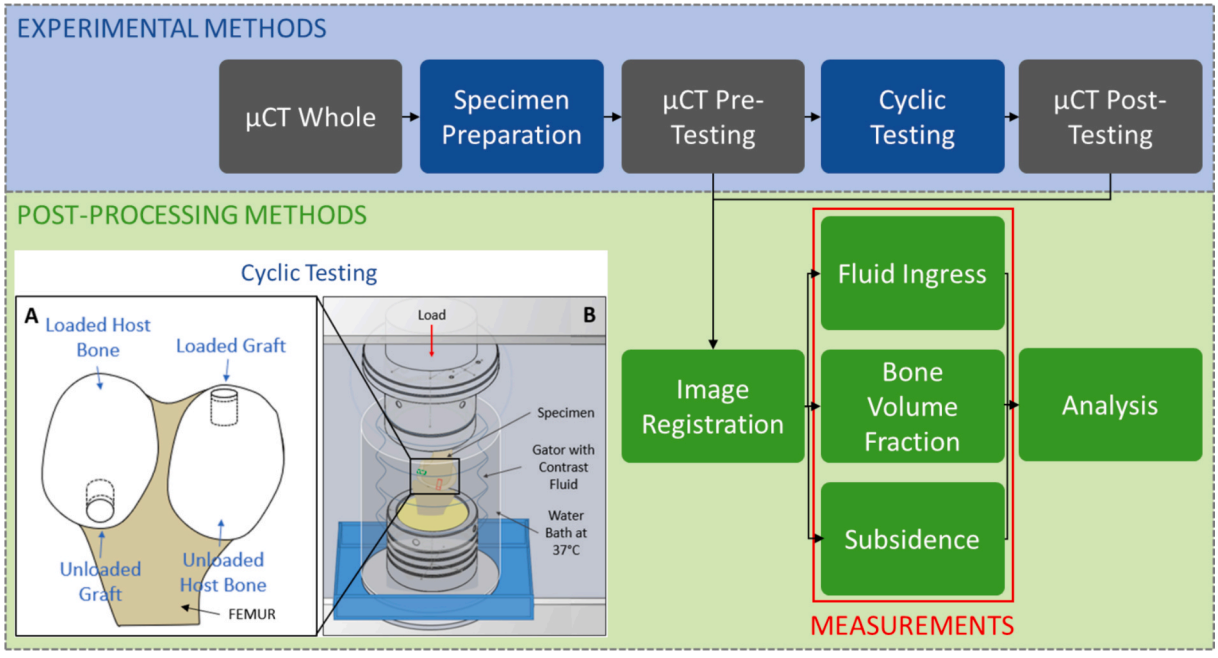

Fig. 1. Flow diagram of experimental and post-processing methodology. Inset shows details of the cyclic testing: [A] Prepared specimen with six sites of interest. "loaded graft-host interface" at the interface of the loaded graft and host bone; "loaded graft centre" through the middle of the loaded graft; "unloaded graft-host interface" and "unloaded graft centre" at the unloaded graft site; "loaded host bone" at a location experiencing load but where no graft was implanted; and "unloaded host bone" at an unloaded site where no graft was implanted. [B] Experimental test diagram showing a prepared specimen within testing apparatus, surrounded by a gaiter containing contrast fluid and a water bath at 37 °C.

by the Institute of Orthopaedics and Musculoskeletal Science, University College London.

Grafts were implanted in porcine or ovine tibiofemoral specimens. Skeletally immature (4 to 6 months) porcine tissue was obtained from the food chain within 24 h of slaughter (John Penny & Sons, Leeds, UK). Skeletally mature (6 years +) ovine tissue was harvested from sheep that were used as part of an *in vivo* study for a spinal intervention with return to normal activity (approved by the NAMSA Ethical Committee on January 4, 2016). The ovine tissue was also collected within 24 h of slaughter (sacrificed at the University of Nottingham) under appropriate UK Home Office licenses. Data was collected from three groups [N = 5 per group] (Table 1). Natural porcine osteochondral grafts were implanted in porcine (P) and ovine (O) host bone. Biomimetic constructs (B) were implanted in porcine host bone.

2.3. Experimental methods

Knee specimens were prepared for testing by potting the femoral and tibial shafts in poly-methyl methacrylate (PMMA) cement. The joint capsule was fully intact and was positioned in full extension, using a custom rig that allowed the natural relative position of the femur and tibia to be reproduced following dissection. The rig also allowed the specimen to be fixed within testing apparatus, ensuring natural axial force transmission through the joint during testing.

Following potting, the knees were further dissected to only retain the bones and cartilage. Two defect holes were created in the femoral component with a surgical drill bit to create recipient sites (Fig. 1[A]). For the natural grafts, two porcine osteochondral grafts were implanted; for the biomimetic specimens, two constructs were implanted. A "loaded graft" was implanted axially with the loading direction at the point of initial contact of the femur and tibia, which was typically on the medial condyle. An "unloaded graft" was implanted on a portion of the opposite condyle that would not experience direct loading during testing. While the natural and biomimetic grafts differed in diameter, the diameters of both grafts were 0.15 mm oversized with respect to the recipient site. Clinically, grafts are usually implanted perpendicular to the cartilage surface, to restore surface congruency (Branam and Saber, 2023). However, grafts were implanted axially with respect to the loading direction during experimental testing to ensure axial loading, which resulted in grafts that were not always perpendicular to the cartilage surface.

Specimens were imaged prior to dissection ("whole"), post-preparation but prior to testing ("pre-testing"), and immediately following testing ("post-testing"), using an isotropic resolution of 82 μm (60 kVp and 900 μA), in a high-resolution peripheral-qCT scanner (XtremeCT, Scanco Medical, Switzerland).

Experimental testing consisted of loading the specimen with a uniaxial loading profile of the axial joint reaction force experienced during gait, derived from knee simulators studies (Liu et al., 2015), for 5,000 cycles (1 Hz), using an ElectroPuls® E10,000 (10 kN load cell, Instron, USA) (Fig. 1[B]). Testing ran between 0 N and peak axial loads of 1,000 N for porcine host bone (Liu et al., 2015; Liu et al., 2019), and 1,300 N for ovine host bone (Taylor et al., 2011).

During testing, the specimen was housed in a gaiter containing a contrast fluid (Fig. 1[B]); the fluid was heated to 37 °C with an external water bath to replicate the *in vivo* environment. By performing the testing in the presence of a contrast fluid, the fluid ingress could be visualised by the change in brightness of individual voxels between pre- and post-testing μCT scans. An in-house contrast analysis was undertaken to develop a suitable contrast fluid, based on previous work (Bint-E-Siddiq, 2019), using Sodium Iodide (NaI) as a contrast agent, also ensuring that the contrast fluid did not damage the biomimetic constructs. A suitable concentration was determined for this application containing 0.8 M NaI in PBS.

2.4. Post-Processing methods

Fluid ingress, graft subsidence and specimen bone volume fraction were measured from μCT scans for each specimen type (using 32-bit uncompressed DICOMS files), at sites with and without grafts present and that did or did not experience loading during testing.

The μCT scans taken pre- and post-testing were registered using landmarks and automation in Simpleware™ ScanIP (2018; Synopsys, Inc., Mountain View, USA). Individual fluid ingress measurements were

Table 1
Specimen group descriptions.

Group Name	Host Bone Species	Host Site Diameter (mm)	Graft Type	Graft Dimensions (mm)
Porcine (P) [N = 5] **Ovine (O) [N = 5]**	Porcine Ovine	6.35 6.35	Natural Graft: Porcine	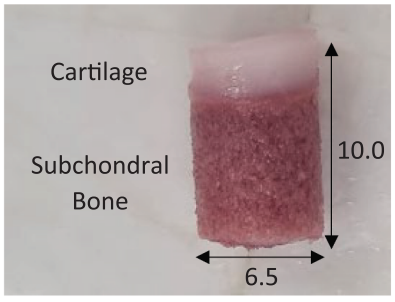
Biomimetic Construct (B) [N = 5]	Porcine	7.35	Layered biomimetic construct	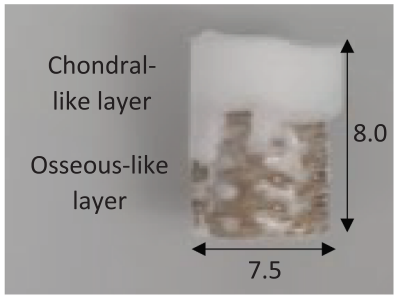

quantified by comparing the greyscale distribution across a line profile between pre- and post-testing μCT scans, where a difference in greyscale value at the same location identified fluid presence. A Matlab script (Matlab R2022a, Mathworks, USA) was written to visualise the greyscale distribution across the line profiles and identify key features: a reference point and a convergence point. The reference point was defined on the pre-testing μCT line profile, where the first greyscale value became positive. The convergence point was defined where the two line profiles converged (difference in greyscale ≤ 0), as the location where the fluid penetrated the tissue. Fluid ingress was identified as the distance between the reference point and the convergence point (Fig. 2). A Gaussian smoothing filter, with a kernel size of seven based on sensitivity testing (Supplementary Data – Section B), was used to minimise the effect of noise in the greyscale profiles. To ensure fluid ingress was accurately calculated, the smoothed data was used to identify the area of convergence, but the actual fluid ingress value was selected from the original data at a position within ± 3 pixels of the convergence point.

Six sites of interest were identified on each specimen, at which fluid ingress was derived (Fig. 1[A]) – two at the loaded graft site, at the interface of the graft and host bone and at the centre of the graft ("Loaded Graft-Host Interface", "Loaded Graft Centre"), two at the unloaded graft site ("Unloaded Graft-Host Interface", "Unloaded Graft Centre"), one at a location experiencing load but where no graft was implanted ("Loaded Host Bone"), and one at an unloaded site where no graft was implanted ("Unloaded Host Bone"). Each value was an average of multiple measurements to represent variations within each site of interest (Supplementary Data – Section B).

Fluid ingress results were normalised with respect to the specimen-specific fluid ingress at the unloaded host bone site. As not all the data for the six sites of interest followed a normal distribution (Shapiro Wilk test), statistical significance between testing groups was determined using a Friedman's test and paired statistical significance between sites of interest was identified using a two-way Dunn's test with a Bonferroni adjustment. All statistical analysis was conducted using SPSS Statistics (Version 29.0, IBM Corp., USA) and a significance level $\alpha = 0.05$.

To investigate whether it influenced fluid ingress, graft subsidence was measured from μCT scans. For each loaded graft and biomimetic construct, subsidence was measured as the axial displacement at the centre of the graft between pre- and post-testing μCT images (Fig. 3). Subsidence was measured at two locations along the length of the graft: the articular cartilage-subchondral bone boundary, and the base of the subchondral bone. It was not appropriate to use the external articular cartilage surface to measure subsidence between scans as the articular cartilage was sometimes flattened following testing or enlarged due to fluid absorption. Any difference that was equivalent to less than one pixel was said to be zero.

To investigate whether fluid ingress is related to bone architecture, the bone volume fraction (BV/TV) was calculated at the unloaded host bone sites of all specimens. The difference in bone volume fraction between graft and host bone sites was also calculated and compared to the fluid ingress at graft-host interfaces. Bone volume fraction was calculated from pre-testing μCT scans for cylindrical regions of interest with a diameter half that of the bone graft (8.0 mm length and 3.175 mm diameter) (Fig. 3). The bone region was manually determined visually to produce a threshold that appropriately separated the bone and interstitial space. This threshold was then used consistently within the same species, but a different threshold was used for different species. Bone volume fraction was calculated as the ratio of bone volume to total volume (BV/TV).

3. Results

Visual analysis of post-testing μCT scans of each porcine (P) or ovine (O) specimen allowed identification of subsidence (O2), subchondral bone damage (P2), fluid pooling below grafts (P2, O4, B1), delamination of the articular cartilage following testing (O1, O3), and orientation of the recipient sites (4.3 ± 1.6°) (Fig. 4; Supplementary Data - Section C). In some porcine specimens (P3, P5), channels in the subchondral bone were observed on the μCT scans that promoted fluid ingress throughout the specimen, resulting in a lack of variation in recorded fluid ingress between sites of interest.

Graft presence and loading had significantly greater fluid ingress compared to unloaded host bone sites (Fig. 5). The fluid ingress at each site of interest for each specimen is given with respect to the average fluid ingress at the unloaded host bone site of each specimen which was generally larger in the porcine host bone than the ovine host bone (P = 17.7 mm, O = 2.6 mm, B = 10.2 mm). Pairwise statistical analysis results are presented in Table 2.

Subsidence was detected in nine specimens in total, with a maximum subsidence of 1.1 mm observed (O2). Non-zero subsidence values at the bone base location [n = 6] were compared to corresponding relative fluid ingress values (Supplementary Data – Section D) but presented no clear relationship with fluid ingress.

There was a broad trend ($R^2 = 0.57$; $p < 0.05$) of reducing fluid ingress with increasing bone volume fraction at host bone sites (Fig. 6).

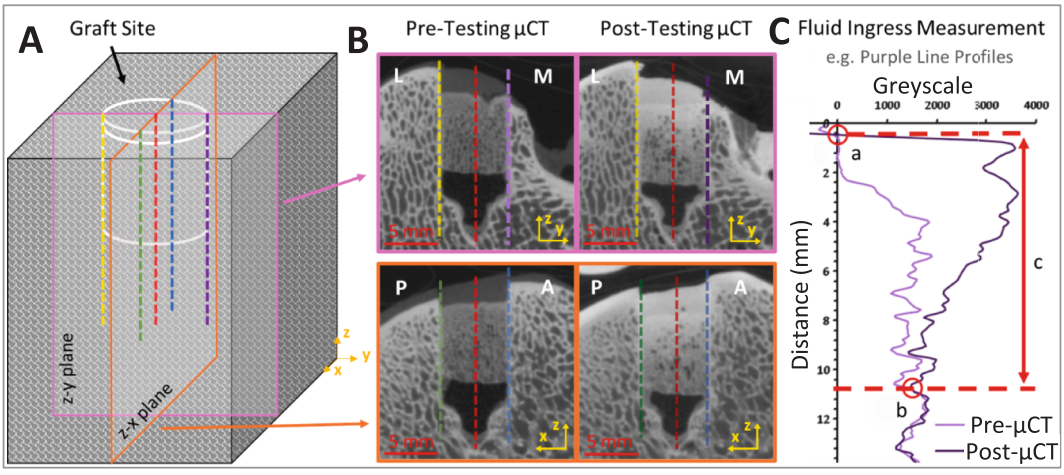

Fig. 2. Post-processing: Fluid ingress calculation at a graft site. [A] Fluid ingress as an average of measurements within each site of interest; [B] Line profiles identified on pre- and post-testing μCT scans; [C] An example of a single fluid ingress measurement for a line profile with (a) reference point identified as the first pre-testing μCT raw value to become positive, (b) convergence point identified as the first point where the difference between greyscales is less than zero, (c) fluid ingress calculated as the difference between reference and convergence points.

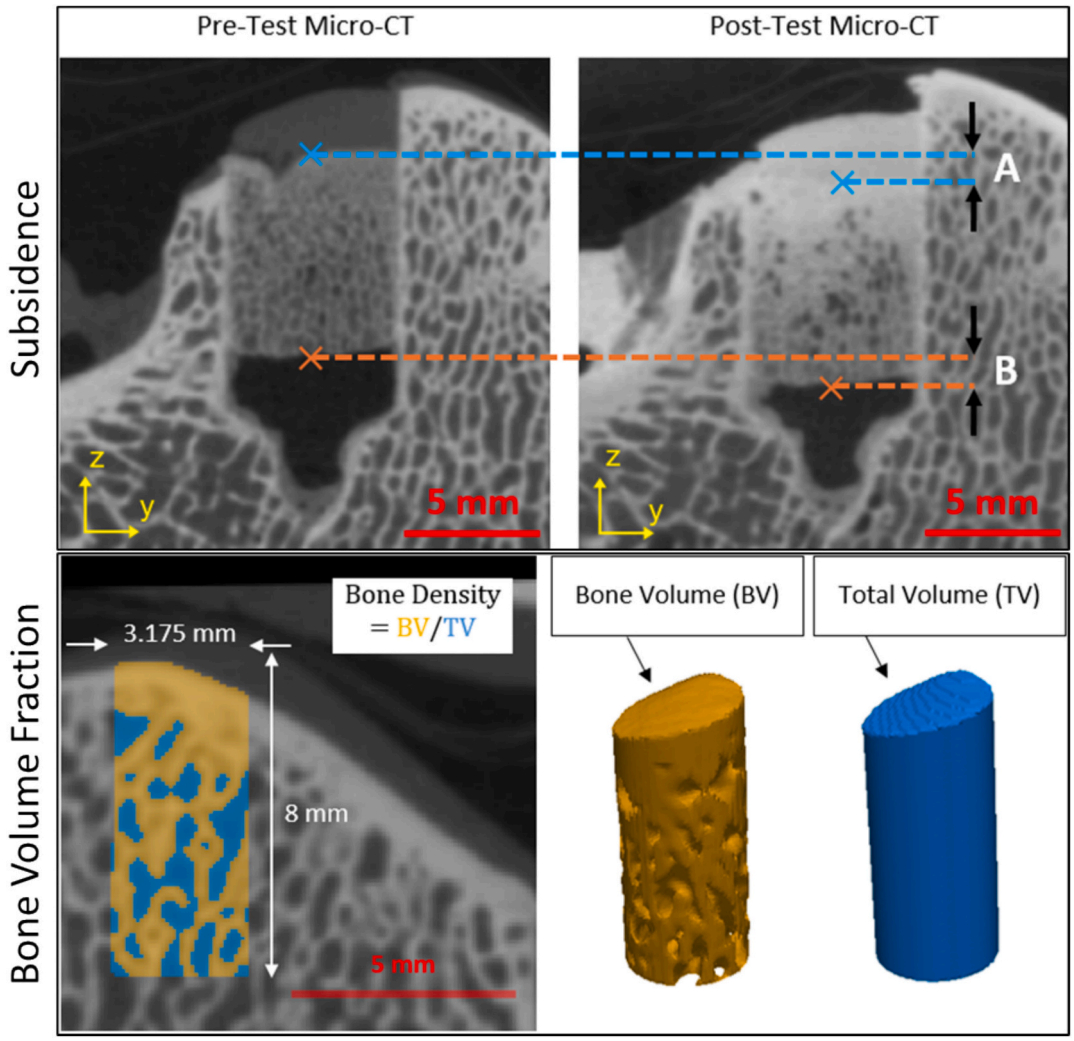

Fig. 3. Experimental outputs of subsidence and bone volume fraction calculated from μCT scans. Subsidence measurements taken between pre- and post-testing μCT scans. Taken from each loaded graft (A) centrally at the top of the subchondral bone and (B) centrally at the base of the subchondral bone. Bone volume fraction measurement. Cylindrical masks (half the diameter of graft sites) of bone volume (BV) and total volume (TV) at the unloaded host bone site used to calculate bone volume fraction (BV/TV).

In general, the BV/TV of ovine host bone was larger (0.82 ± 0.07) than the porcine host bone (P specimens: 0.50 ± 0.13, B specimens: 0.57 ± 0.16). There was a weak correlation ($R^2 = 0.33$; $p < 0.05$) between the ratio of bone volume fraction at graft and host sites, and fluid ingress at graft-host interfaces, where fluid ingress tended to reduce as the bone volume fraction of the graft tended towards the bone volume fraction of the host (Fig. 7).

4. Discussion

The purpose of this study was to develop a method to study the early mechanical performance of osteochondral bone grafts in a controlled *in vitro* experiment in porcine and ovine pre-clinical models. Specifically, the aim was to examine the potential for fluid ingress, which has been linked to cyst formation, and early graft subsidence in the period before any osseointegration has occurred. This work demonstrated that the presence of a graft and loading both increased fluid ingress into osteochondral tissue and highlighted the influence of graft and host bone properties in limiting fluid ingress.

The skeletally immature porcine tissue (low mineralisation, low stiffness) and skeletally mature ovine tissue (high mineralisation, high stiffness, more brittle) represented a range of bone properties. Similarly, the choice of natural grafts and biomimetic constructs represented what can be used clinically. The mismatch of materials at graft-host interfaces represented where material properties can differ clinically, for example by adopting allografts or decellularized grafts.

In terms of limitations, it was difficult to prepare specimens exactly as theorised, for example creating a perfectly axial graft site to a perfectly bottomed depth. This resulted in loading not always being entirely axial to the graft (4.3 ± 1.6°). However, this demonstrates the clinical challenge of performing osteochondral graft surgery as intended.

Joint loading was simplified to uniaxial loading which is not entirely representative of the *in vivo* environment. However, this was deliberate, to simplify loading, making the test reproducible, with a focus on simulating the pumping action of a graft *in vivo*. The effect of shear loading on fluid ingress was not captured. This could be done in the future with a similar method used with full joint simulation, with the additional benefit not to require axial implantation of grafts.

For bone volume fraction measurements calculated from pre-test μCT scans, it was observed that a single threshold value did not always accurately capture the trabecular structure between specimens of the same species, likely due to differences in tissue mineralisation between specimens. It may therefore be more appropriate to use inconsistent thresholds within each species, dependant on the region of interest. Also, fluid ingress at the top of the subchondral bone often made it

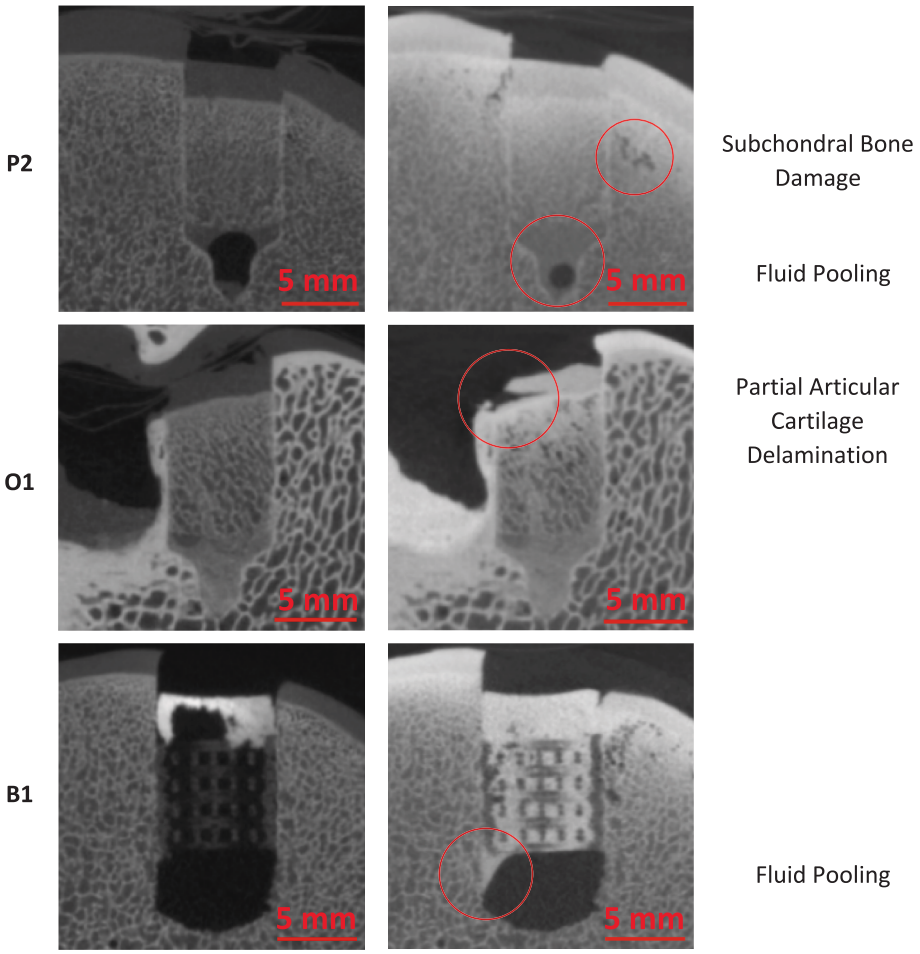

Fig. 4. Visual analysis of μCT scans allowing visualisation of subchondral bone damage (P2), fluid pooling below grafts (P2, B1) and delamination of articular cartilage following testing (O1).

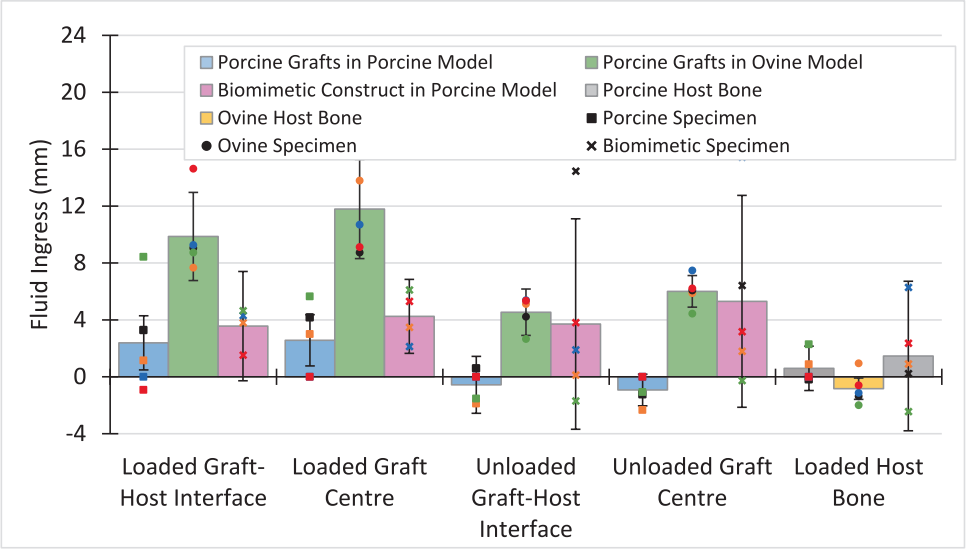

Fig. 5. Relative fluid ingress results with respect to each specimen's unloaded host bone site (average fluid ingress at unloaded host bone site for P = 17.7 mm, O = 2.6 mm, B = 10.2 mm).

difficult to identify the articular cartilage-bone boundary in the post-test μCT scan, limiting the subsidence measurements that could be obtained at this point.

Graft sites, particularly loaded graft sites, produced significantly greater fluid ingress compared to the unloaded host bone, indicating that the presence of osteochondral grafts increased fluid ingress. With fluid sometimes present in the interstitial space below grafts following testing, it appeared that pressure on the fluid from the loaded graft

Table 2
Statistical significance: Statistical significance was identified using a Friedman test ($p = 0.0001948$). Pairwise statistical significance was calculated using a post hoc Dunn's test and statistical significance indicated with an adjusted Bonferroni correction applied, resulting in an adjusted significance value of $p < 0.003$.

	Loaded Graft-Host Interface	Loaded Graft Centre	Unloaded Graft-Host Interface	Unloaded Graft Centre	Loaded Host Bone
Loaded Graft-Host Interface		0.419	0.015	0.106	0.003
Loaded Graft Centre	0.419		0.001	0.015	<0.001
Unloaded Graft-Host Interface	0.015	0.001		0.419	0.614
Unloaded Graft Centre	0.106	0.015	0.419		0.189
Loaded Host Bone	0.003	<0.001	0.614	0.189	
Unloaded Host Bone	0.001	<0.001	0.419	0.106	0.762

promoted further ingress into the subchondral bone.

Loading alone tended to increase fluid ingress, though a combination of loading and graft presence promoted ingress the most. This suggests that the repeated loading overcomes the natural structural barriers to fluid movement and, given the loads in this study represented those experienced during gait, supporting existing clinical protocols to avoid weight bearing activities for a minimum of eight weeks following surgery (Haber et al., 2019). At graft sites, this effect was most evident for the porcine grafts in ovine host bone specimens where there was a mismatch in the trabecular structure between the host and graft, while the porcine grafts in porcine bone appeared to most closely match ingress naturally through the host bone. This suggests that matching the material and structural properties of the graft and host may be effective at limiting fluid ingress.

There was greater difference in fluid ingress between regions with and without grafts in the porcine graft in ovine bone samples than the biomimetic constructs or porcine grafts in porcine bone. This may indicate that the constructs provide a good match of structural and mechanical properties to the porcine host bone or that host bone properties are a more significant factor in indicating fluid ingress than graft properties. Previous research suggested that the stability of osteochondral grafts is driven by the host bone quality (Casper-Taylor et al., 2019).

Without grafts or loading, there was more fluid ingress in the porcine model than in the ovine model. With large differences between the fluid ingress in the unloaded host bone between species, this was theorised to be a result of differences in trabecular structure and bone density that exist in different animal models. Previous studies identified differences in bone density and mechanical stiffness of porcine and ovine vertebral specimens (Zapata-Cornelio et al., 2017). When investigated, there was a broad trend of increasing bone volume fraction with reduced fluid ingress (Fig. 6) at host bone sites which was largely species driven.

However, the trend were not strong correlations ($R^2 = 0.57$), suggesting BV/TV does not consider enough of the structural and mechanical properties to be used as an indicator for fluid ingress. As well as bone volume fraction, other material property differences exist between animal models. For example, porcine bone is softer and less mineralised and, while ovine and porcine have similar trabecular spacing, ovine bone has higher average and maximum trabecular thicknesses. This difference in material properties may result in different effects at graft-host interfaces during graft implantation. Brittle trabeculae (more likely for ovine bone) may fracture while more elastic bone (more likely for porcine bone) may deform in response to graft implantation which would result in structurally different graft-host interfaces. There was also more variation in bone volume fraction in the porcine host bone than the ovine host bone. Despite sharing structural features with human tissue, animal models also differ to human bone. One study showed the bone plates of several animal models (including sheep) were thicker than human bone plates with denser and thicker trabeculae (Chevrier et al., 2015).

Additionally, a greater the ratio of bone volume fraction between graft and host materials correlated with a reduction in fluid ingress at the graft host interface, suggesting developers of biomimetic constructs should seek to match the mechanical properties to that of the intended host bone to limit fluid ingress (Fig. 7).

Approximately eight of 15 loaded graft sites had a space below the graft (unbottomed), which tended to increase subsidence at the bone top. This supports existing clinical preference to use bottomed grafts, with the subsidence of unbottomed grafts also observed clinically (Kock et al., 2011; Bowland et al., 2019). Less subsidence was seen at the base

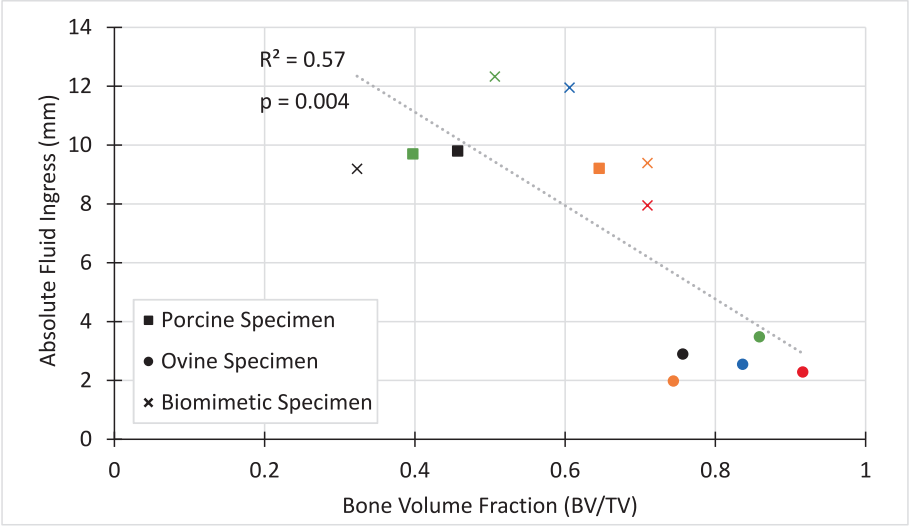

Fig. 6. Evaluation of bone volume fraction (BV/TV) against absolute fluid ingress (mm) at unloaded host bone sites of all specimens (except P3 and P5 due to their absolute fluid ingress measurements equalling zero).

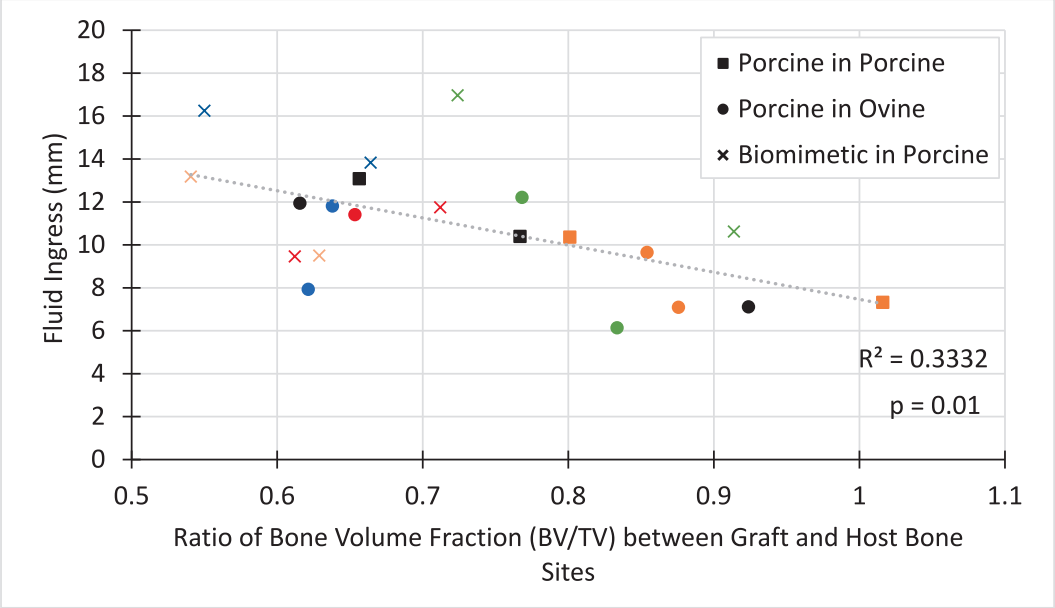

Fig. 7. Ratio between graft and host bone volume fraction (BV/TV) against absolute fluid ingress (mm) at loaded and unloaded graft-host interface sites on all specimens (except P3 and P5 due to their absolute fluid ingress measurements equalling zero). (Note: Ratio < 1 when graft BV/TV < host BV/TV).

of the grafts compared to the top due to partial compression of the grafts.

While graft presence and loading were shown to promote fluid ingress, further links need to be made between fluid ingress and cyst development to validate this theory. Going forward, this method can be translated to cadaveric human tissue and used to investigate the effect of clinical variables such as graft type and surgical technique. The methodology enables evaluation of other factors such as the effect of limiting weight bearing activities before graft integration with bone by assessing the effect of lower loads, or understanding the effect of shear or graft size, by investigating these parameters systematically.

5. Conclusion

A novel method was developed to measure subsidence and fluid ingress over multiple loading cycles to evaluate osteochondral grafting *in vitro*.

A significant increase in fluid ingress was observed from a combination of graft presence and following loading. This finding suggests that limiting fluid ingress at graft-host interfaces may be key to reducing the incidence of cyst development, alongside other surgical features such as graft oversizing, which have previously been shown to reduce subsidence.

Mechanisms of cyst formation associated with fluid ingress are shown to be exacerbated by loading with a dependence on graft and host material properties, especially host bone quality, which has previously been linked to graft stability. The success of biomimetic constructs may be driven by matching the material's mechanical properties with the host bone. Clinicians are also encouraged to consider host bone quality when assessing a patient's suitability for surgery.

This study provides a novel methodology for the pre-clinical assessment of grafts with the potential for translation to human tissue and other pre-clinical applications.

Funding statement

The study was supported by the Engineering and Physical Sciences Research Council (EPSRC) through EP/T517860/1. RW is supported in part by the National Institute for Health and Care Research (NIHR) Leeds Biomedical Research Centre (BRC) (NIHR203331). MM is supported in part by the EPSRC through an Open Fellowship (EP/X032183/1).

CRediT authorship contribution statement

Lara Esquivel: Writing – review & editing, Writing – original draft, Visualization, Software, Methodology, Investigation, Formal analysis, Data curation, Conceptualization. **Mingjing Zhang:** Writing – review & editing, Resources, Methodology, Conceptualization. **Gavin Day:** Writing – review & editing, Supervision, Resources, Methodology, Formal analysis, Conceptualization. **Marlène Mengoni:** Writing – review & editing, Supervision, Methodology, Funding acquisition, Formal analysis, Conceptualization. **Hazel Fermor:** Writing – review & editing, Supervision, Methodology, Formal analysis, Conceptualization. **Chaozong Liu:** Writing – review & editing, Resources, Methodology, Conceptualization. **Ruth Wilcox:** Writing – review & editing, Supervision, Methodology, Funding acquisition, Formal analysis, Conceptualization.

Declaration of competing interest

The authors declare that they have no known competing financial interests or personal relationships that could have appeared to influence the work reported in this paper.

Appendix A. Supplementary data

Supplementary data to this article can be found online at https://doi.org/10.1016/j.jbiomech.2025.113132.

References

Ackermann, J., Duerr, R.A., Barbieri Mestriner, A., Shah, N., Gomoll, A.H., 2019a. Effect of Graft-Host Interference Fit on Graft Integration after Osteochondral Allograft Transplantation: a Comparative MRI Analysis of two Instrumentation Sets. Cartilage 13 (1 Suppl), 920S.

Ackermann, J., Merkely, G., Shah, N., Gomoll, A.H., 2019b. Decreased Graft Thickness is Associated with Subchondral Cyst Formation after Osteochondral Allograft Transplantation in the knee. Am. J. Sports Med. 47 (9), 2123–2129.

Ackermann, J., Mestriner, A.B., Shah, N., Gomoll, A.H., 2019c. Effect of Autogenous Bone Marrow Aspirate Treatment on magnetic Resonance Imaging Integration of

Osteochondral Allografts in the knee: a Matched Comparative Imaging Analysis. Arthroscopy J. Arthrosc. Relat. Surg. Off. Publicat. Arthroscopy Assoc. North Am. Int. Arthrosc. Associat. 35 (8), 2436–2444.
Aerssens, J., Boonen, S., Lowet, G., Dequeker, J., 1998. Interspecies differences in Bone Composition, Density, and Quality: potential Implications for in Vivo Bone Research. Endocrinology 139 (2), 663–670.
Beck, A., Murphy, D.J., Carey-Smith, R., Wood, D.J., Zheng, M.H., 2016. Treatment of Articular Cartilage Defects with Microfracture and Autologous Matrix-Induced Chondrogenesis leads to Extensive Subchondral Bone Cyst Formation in a Sheep Model. Am. J. Sports Med. 44 (10), 2629–2643.
Bint-E-Siddiq, A. 2019. Mechanical Characterisation and Computational Modelling of Spinal Ligaments.
Bowland, P., Cowie, R.M., Ingham, E., Fisher, J., Jennings, L.M., 2019. Biomechanical assessment of the stability of osteochondral grafts implanted in porcine and bovine femoral condyles. Proc. Inst. Mech. Eng. 234 (2), 163–170.
Branam, G. and Saber, A. 2023. *Osteochondral Autograft Transplantation* [Online]. StatPearls [Internet]. Treasure Island (FL): StatPearls Publishing. [Accessed 20 March 2025]. Available from: https://pubmed.ncbi.nlm.nih.gov/32809490/.
Casper-Taylor, M.E., Wilcox, R., Mengoni, M., 2019. Stiffness of subchondral bone of grafts and defect site in osteochondral repair influences stability of repair. Osteoarthr. Cartil. 27, S160.
Chen, H., Hoemann, C.D., Sun, J., Chevrier, A., McKee, M.D., Shive, M.S., Hurtig, M., Buschmann, M.D., 2011. Depth of subchondral perforation influences the outcome of bone marrow stimulation cartilage repair. J. Orthop. Res. 29 (8), 1178–1184.
Chevrier, A., Kouao, A.S.M., Picard, G., Hurtig, M.B., Buschmann, M.D., 2015. Interspecies comparison of subchondral bone properties important for cartilage repair. J. Orthop. Res. 33 (1), 63–70.
Davis, S., Roldo, M., Blunn, G., Tozzi, G., Roncada, T., 2021. Influence of the Mechanical Environment on the Regeneration of Osteochondral Defects. Front. Bioeng. Biotechnol. 9, 603408.
Gao, L., Cucchiarini, M., Madry, H., 2020. Cyst formation in the subchondral bone following cartilage repair. Clin. Transl. Med. 10 (8), e248.
Haber, D.B., Logan, C.A., Murphy, C.P., Sanchez, A., LaPrade, R.F., Provencher, M.T., 2019. Osteochondral allograft transplantation for the knee: post-operative rehabilitation. Int. J. Sports Phys. Ther. 14 (3), 487.
Hoveidaei, A.H., Ghaseminejad-Raeini, A., Esmaeili, S., Sharafi, A., Ghaderi, A., Pirahesh, K., Azarboo, A., Nwankwo, B.O., Conway, J.D., 2024. Effectiveness of synthetic versus autologous bone grafts in foot and ankle surgery: a systematic review and meta-analysis. BMC Musculoskelet. Disord. 25 (1), 539.
Juels, C.A., So, E., Seidenstricker, C., Holmes, J., Scott, R.T., 2020. Complications of En Bloc Osteochondral Talar Allografts and Treatment of failures: Literature Review and Case Report. J. Foot Ankle Surg. Off. Publicat. Am. Coll. Foot Ankle Surg. 59 (1), 149–155.
Kock, N.B., Hannink, G., van Kampen, A., Verdonschot, N., van Susante, J.L.C., Buma, P., 2011. Evaluation of subsidence, chondrocyte survival and graft incorporation following autologous osteochondral transplantation. Knee Surg., Sports Traumatol. Arthrosc. Off. J. ESSKA. 19 (11), 1962–1970.
Liu, A., Ingham, E., Fisher, J., Jennings, L.M., 2019. Development of a pre-clinical experimental simulation model of the natural porcine knee with appropriate ligamentous constraints. PLoS One 14 (5).
Liu, A., Jennings, L.M., Ingham, E. and Fisher, J. 2015. Tribology studies of the natural knee using an animal model in a new whole joint natural knee simulator.
Marom, N., Bugbee, W., Williams, R.J., 2020. Osteochondral Grafts failures. Operat. Techniq. Spor. Med. 28 (1), 150712.
Meng, X., Ziadlou, R., Grad, S., Alini, M., Wen, C., Lai, Y., Qin, L., Zhao, Y., Wang, X., 2020. Animal Models of Osteochondral defect for Testing Biomaterials. Biochem. Res. Int. 2020 (1), 9659412.
Oláh, T., Cai, X., Michaelis, J.C., Madry, H., 2021. Comparative anatomy and morphology of the knee in translational models for articular cartilage disorders. Part I: Large animals. Ann. Anat. - Anat. Anz. 235, 151680.
Pallante-Kichura, A.L., Cory, E., Bugbee, W.D., Sah, R.L., 2013. Bone cysts after osteochondral allograft repair of cartilage defects in goats suggest abnormal interaction between subchondral bone and overlying synovial joint tissues. Bone 57 (1), 259–268.
Shimozono, Y., Hurley, E.T., Nguyen, J.T., Deyer, T.W., Kennedy, J.G., 2018. Allograft Compared with Autograft in Osteochondral Transplantation for the Treatment of Osteochondral Lesions of the Talus. J. Bone Joint Surg. Am. 100 (21), 1838–1844.
Shimozono, Y., Yasui, Y., Hurley, E.T., Paugh, R.A., Deyer, T.W., Kennedy, J.G., 2019. Concentrated Bone Marrow Aspirate May Decrease Postoperative Cyst Occurrence Rate in Autologous Osteochondral Transplantation for Osteochondral Lesions of the Talus. Arthroscopy J. Arthrosc. Related Surg. Off. Publicat. Arthrosc. Associat. North Am. Int. Arthrosc. Associat. 35 (1), 99–105.
Solanki, K., Shanmugasundaram, S., Shetty, N., Kim, S.J., 2021. Articular cartilage repair & joint preservation: a review of the current status of biological approach. J. Clin. Orthopaed. Traum. 22.
Suderman, R.P., Hurtig, M.B., Grynpas, M.D., Kuzyk, P.R.T., Changoor, A., 2024. Effect of Press-Fit size on Insertion Mechanics and Cartilage Viability in Human and Ovine Osteochondral Grafts. Cartilage.
Taylor, W.R., Poepplau, B.M., König, C., Ehrig, R.M., Zachow, S., Duda, G.N., Heller, M. O., 2011. The medial–lateral force distribution in the ovine stifle joint during walking. J. Orthop. Res. 29 (4), 567–571.
Vachon, A., Bramlage, L.R., Gabel, A.A., Weisbrode, S., 1986. Evaluation of the repair process of cartilage defects of the equine third carpal bone with and without subchondral bone perforation. Am. J. Vet. Res. 47 (12), 2637–2645.
Wang, W., Ding, R., Zhang, N., Hernigou, P., 2021. Subchondral bone cysts regress after correction of malalignment in knee osteoarthritis: comply with Wolff's law. Int. Orthop. 45 (2), 445–451.
Zapata-Cornelio, F.Y., Day, G.A., Coe, R.H., Sikora, S.N.F., Wijayathunga, V.N., Tarsuslugil, S.M., Mengoni, M., Wilcox, R.K., 2017. Methodology to produce Specimen-specific Models of Vertebrae: Application to Different Species. Ann. Biomed. Eng. 45 (10), 2451.
Zeng, J.H., Liu, S.W., Xiong, L., Qiu, P., Ding, L.H., Xiong, S.L., Li, J.T., Liao, X.G., Tang, Z.M., 2018. Scaffolds for the repair of bone defects in clinical studies: a systematic review. J. Orthop. Surg. Res. 13 (1), 1–14.
Zheng, J., Zhao, H., Ouyang, Z., Zhou, X., Kang, J., Yang, C., Sun, C., Xiong, M., Fu, M., Jin, D., Wang, L., Li, D., Li, Q., 2022. Additively-manufactured PEEK/HA porous scaffolds with excellent osteogenesis for bone tissue repairing. Compos. B Eng. 232, 109508.